CINTAL - Centro de Investigação Tecnológica do Algarve
Universidade do Algarve

Basin scale simulations of Ocean Acoustic Tomography in the Portuguese Exclusive Economic Zone

ATOMS Project

O.C. Rodríguez

Rep. 03/02 - SiPLAB
16/October/2002

University of Algarve
Campus da Penha
8005-139, Faro,
Portugal

tel: +351-289800131
fax: +351-289864258
cintal@ualg.pt
www.ualg.pt/cintal

Work requested by	CINTAL Universidade do Algarve, Campus da Penha, 8005-139, Faro, Portugal tel: +351-289800131, cintal@ualg.pt, www.ualg.pt/cintal
Laboratory performing the work	SiPLAB - Signal Processing Laboratory Universidade do Algarve, FCT, Campus de Gambelas, 8000 Faro, Portugal tel: +351-289800949, info@siplab.uceh.ualg.pt, www.ualg.pt/uceh/adeec/siplab
Projects	ATOMS - FCT, PDCTM/P/MAR/15296/1999
Title	Basin scale simulations of Ocean Acoustic Tomography in the Portuguese Exclusive Economic Zone
Authors	O.C.Rodríguez
Date	October 16, 2002
Reference	03/02 - SiPLAB
Number of pages	37 (thirty seven)
Abstract	This internal report describes some of the experiments developed in the field of Ocean Acoustic Tomography, simulation results regarding the acoustic monitoring of the Portuguese Economic Exclussive Zone and a brief description of binary m-sequences.
Clearance level	UNCLASSIFIED
Distribution list	CINTAL(1), SiPLAB(1), FCT(1)
Total number of copies	3 (three)

intentionally blank

Contents

List of Figures **V**

1 Introduction **7**

2 Bibliographic review **8**
2.1 Sound propagation in the ocean 8
2.1.1 Planetary scales 8
2.1.2 Sub-basin scales 8
2.2 Ocean Tomography 9
2.2.1 Mesoscale 9
2.2.2 Sub-basin scales 10
2.2.3 Basin scales 10
2.2.4 Small (coastal) scales 11

3 Simulations **13**
3.1 The Portuguese EEZ 13
3.2 Oceanographic data and bathymetry 13
3.3 Range independent simulations 18
3.3.1 Sound speed profile 18
3.3.2 Source positioning 21
3.3.3 Receiver positioning 21
3.3.4 Ray tracing 21
3.3.5 Sound speed parameterization 22
3.3.6 Inversion results 22
3.4 Range dependent simulations 23

4 Conclusions **28**

I M-sequences **31**
I.1 Preliminary definitions 31
I.2 Coefficients of m-sequences 32
I.3 Signal modulation based on m-sequences 33

II Primitive polynomials **35**

List of Figures

2.1 General overview of the receiving array at the Pioneer Seamount. 11

2.2 General overview of the experimental site during the Barents Sea Polar Front Tomography Experiment. 12

3.1 General overview of the Portuguese EEZ. 14

3.2 Portuguese EEZ bathymetry and selected transects T1, T2 and T3. 14

3.3 Sound speed distributions: (a) T1; (b) T2; (c) T3. 15

3.4 Transects bathymetry: (a) T1; (b) T2; (c) T3. In all cases range increases towards mainland Portugal, with range "0" corresponding to longitude -30°. 16

3.5 Normalized distribution of eigenvalues for T1 (continuous line), T2 (dot-dashed line) and T3 (dashed line). 17

3.6 Mean sound speed profile $c_0(z)$ for T1: (a) mean average of available data; (b) corresponding Munk extrapolation up to the maximum depth. 19

3.7 Extrapolated range-dependent sound speed distribution $c(z, r)$ along T1 (case (a)) and expected sound speed perturbation $\delta c(z, r)$ (case (b)). . . . 20

3.8 Ray depth distribution $\zeta(\theta, R)$ for $\theta \in [-20°, 20°]$, at $R = 50$ km (case (a)) and $R = 1000$ km (case (b)). 24

3.9 Perturbed sound speed profile $c(z)$ for T1: (a) Munk extrapolation at the deepest site of T1; (b) corresponding sound speed perturbation $\delta c(z) = c(z) - c_0(z)$. 25

3.10 (a) Some stable eigenrays, the circles indicate the position of the source and the receiver; (b) temporal dispersion of arrivals. 26

3.11 Expected perturbation of sound speed $\delta c(z)$ (dashed line) and estimate (continuous line). 27

6.1 Dependence of the number of primitive polynomials, N, on the polynomials order, r. 35

intentionally blank

Chapter 1

Introduction

The main purpose of this internal report consists in developing a general and brief discussion of technical and experimental techniques of Ocean Acoustic Tomography, followed by a simulated study of application in the sub-basin of the Portuguese Exclusive Economic Zone (hereafter called as the Portuguese EEZ), lasting between mainland Portugal and the Açores and Madeira archipelagos. The discussion will be based on a bibliographic review, regarding proposed and/or experimental applications of Ocean Acoustic Tomography to the monitoring of small (coastal), mesoscale, sub-basin and basin areas of the ocean, corresponding to around 10 km, 100 km, 1 Mm, and more than 1 Mm ranges, respectively. The bibliographical review will be focused on the following items:

- Transmission and propagation geometry: characteristic source/receiver ranges and depths.
- Instrumentation: types of sources, emitted signals and receiving arrays.
- Environmental characterization: types of present ocean phenomena and their influence on the propagating signal.
- Environmental inversion: proposed/used method of inversion for waveguide monitoring and inversion accuracy.

After the discussion of those topics it will follow a simulated study of Ocean Acoustic Tomography applied to the monitoring of the Portuguese EEZ. The instrumentation geometry of the simulated study and the corresponding strategy of environmental inversion will be based partially on the review and partially on historical data from NODC databases. The simulation results, indicating the expected advantages and/or disadvantages of the proposed method of environmental monitoring for the Portuguese EEZ, will be discussed at the end of the report.

Chapter 2

Bibliographic review

Spatial averages of ocean temperature on a large (basin) scale are desirable for the study of ocean climate [1]. However, traditional methods have not given the data required for an understanding of ocean variability at this scale, largely because of the effects of the intense mesoscale variability. The monitoring of large ocean areas based on Ocean Acoustic Tomography has the potential of overcoming many of the technical and economical difficulties that arise from monitoring based on standard "local" and "direct" techniques (like thermistor chains or CTDS), although tomographic observations are not intended to stand alone, but to complement existing data acquired with traditional methods [1]. This chapter will be dedicated to an historical bibliographical overview of experiments dedicated to sound propagation at long ranges, and to proposed and tested applications of Ocean Acoustic Tomography at mesoscale, sub-basin, basin and antipodal scales.

2.1 Sound propagation in the ocean

2.1.1 Planetary scales

The earliest antipodal transmission (range about 20 Mm) took place 21 March 1960, during a geophysical survey [1]. Three 300-pound amatol charges were detonated at 5 min intervals near the sound axis off Perth, Australia, at an approximated depth of 1000 m. The center frequency for the explosive sources was estimated at 15 Hz. The detonations were clearly recorded by two hydrophones off Bermuda, one located at the sound channel (1323 m depth), and the other bottom mounted. Sound transmissions fulfilled a prediction made in 1944 by Ewing and Worzel, leading to the discovery of the SOFAR channel. Although the survey was not designed for tomography purposes the fact that sound transmissions could be detected at planetary scales (between Australia, in the Indian Ocean, and Bermuda, in the Caribbean Sea) constituted an important indicator of the transparency of the ocean channel to sound signals.

2.1.2 Sub-basin scales

One year after the first antipodal transmission Hamilton started the SCAVE (Sound Channel Axis Velocity Experiment) transmissions from Antigua to Bermuda and Eleuthera,

separated by more than 1 Mm. Transmission distances were of the order of 2 Mm. Precisely located and timed SOFAR explosive charges were fired at axial depth off Antigua, and received signals were recorded using the hydrophone array of the Atlantic Missile Range. Three individual hydrophones, separated by 60 km, were placed at Eleuthera. The same receiving system was used off Bermuda although only the acoustic data acquired at the first hydrophone was sufficiently stable for further analysis. Measured travel time variations over 27 months achieved amplitudes up to 200 ms. Once again the experiment was not designed for tomography purposes. However it provided important experimental evidence regarding the stability and resolution of travel time data over long periods of transmission.

2.2 Ocean Tomography

2.2.1 Mesoscale

The 1981 Demonstration Experiment

The first experiment specifically designed for tomography purposes was developed in 1981, by a set of researchers known as the Ocean Tomography Group. The 1981 Demonstration Experiment was designed to monitor a square of 300×300 km^2, in the Hatteras abyssal plain, southwest of Bermuda [1, 2, 3]. Four acoustic sources, moored at a nominal depth of 2000 m along the first vertical side of the square, transmitted phase-coded m-sequences with digits containing 14 cycles of a 224 Hz carrier, with a duration of 62,5 ms. The monitored region has a nominal depth of 5400 m and very small depth variations. The signals were transmitted to a set of 5 receivers moored at the same depth of the sources and distributed along the second side of the square (except one receiver, that was moored on the top side of the square). Travel time data, together with a parameterization of sound speed using Empirical Orthogonal Functions (hereafter EOFs), were further used for a Gauss-Markov inversion procedure[1] [1, 2]. Tomography maps allowed to follow the evolution of the monitored area during three weeks, although the assumed low values of travel time error introduced a large amplitude of error in the estimates.

Matched-Field Tomography

Using travel time data demands the usage of broadband coded source signals, with accurate synchronization of transmission and recordings. High-precision mapping also requires source and receiver positions to be known accurately. In order to overcome those difficulties one could use air-deployed shots, which at low frequencies do not need to be known as accurately as in travel time tomography. Thus, parameterizing sound speed on a EOFs basis could be used to determine the EOFs amplitudes using narrowband estimators [4]. The first experimental demonstration of the method was presented in [5]. Experimental data, from the Pacific Echo Experiment developed in 1986, with an explosive shot source at a range of 53,1 km and 244 m depth was used in combination with a vertical line array, constituted by 16 hydrophones distributed each 45 m between 371 and 1046 m depth. Water depth corresponded to 4100 m. Received signals were processed at a frequency of 15 Hz, allowing to obtain accurate range-independent estimates of sound speed.

[1] This inversion procedure is also known as "stochastic inversion".

2.2.2 Sub-basin scales

Proposals for "El Niño" monitoring

The equatorial Pacific sea surface warming anomaly known as "El Niño" was the subject of widespread interest in the past decade due to its impact on climate variability off the South American coast, in particular, and on the Pacific basin, in general. The El Niño anomaly generally induces a significant overall increase of temperature near the sea surface, between 0 and 8 ° C, extending between 100 and 300 m depth over a range of 2000 km [6, 7]. The first proposal for the acoustic monitoring of El Niño used analytic approximations for the turning depths of eigenrays to predict a variation of ray travel time perturbations up to 180 ms for the temperature variations characteristic of the El Niño. Such amplitudes of ray travel time perturbations were sufficiently large in order to be detected acoustically [6]. An alternative approach, based on acoustic modes, was later proposed in [7]. Briefly, the method was based on the assumption that lower-order modes should get less impact from El Niño, because the energy of those modes should not get into the upper layer significantly. Thus, under the El Niño anomaly some of the acoustic modes will undergo a significant change, which should be reflected on the perturbation of modal travel times [8]. The perturbation on sound speed could be estimated by inverting a system of linear equations, relating the perturbations on modal travel times to sound speed perturbations. Numerical simulations were developed with the KRAKEN model [9]. The experimental geometry corresponded to a water depth of 5000 m, a range of 2000 km and a frequency $f = 10$ Hz. Source depth corresponded to 100 m and the receiving vertical array consisted of a set of hydrophones, equally spaced at every 50 m, with the upper and lower hydrophones at depths of 25 and 275 m, respectively. Predicted modal travel time perturbations for modes 1 to 6 achieved amplitudes up to 529 ms.

2.2.3 Basin scales

The Heard Island Feasibility Test

The Heard Island Feasibility Test took place in 1991 and demonstrated the feasibility of transmissions by non-explosive sources up to antipodal transmissions between 5 and 18 Mm, covering the Indian, Atlantic and Pacific oceans [1]. Transmissions were made from a moving source ship and lasted for only 5 days, thus no having bearing on measuring a variable ocean climate, althoug indicators of ocean warming could be obtained. An important characteristic of the experiment consisted in the usage of several types of m-sequence modulated signals [1, 10] (see appendix I), which allowed to estimate pulse travel times accurately despite the large distances of propagation and allowed to spread the required acoustic energy over a large transmission time minimizing any disturbance to the marine life in the vicinity of the acoustic sources.

The Acoustic Thermometry of Ocean Climate project

Most of the members of the Ocean Tomography Group collaborated in the development of the Acoustic Thermometry of Ocean Climate (ATOC) Project, designed to acquire time series of acoustic travel times over basin-scale paths and using that data to accurately determine range and depth averaged ocean temperature at a range of about 5 Mm [11]–[13]. Acoustic sources were deployed on Pioneer Seamount (see Fig.2.1) near San

Francisco in October 1995 and on the north slope of the Hawaiian island of Kauai in July 1997. Time series of acoustic data of about 15 months duration were obtained from acoustic transmissions from the Pioneer Seamount acoustic source to receiving arrays located throughout the North Pacific ocean, including two moored vertical line arrays of hydrophones (VLAs) and U.S.Navy SOund SUrveilance System (SOSUS) bottom-mounted horizontal line arrays. The acoustic source at the Pioneer Seamount consisted of coded 1023-digit m-sequences, with a 75 Hz carrier frequency and bandwidth of 37,5 Hz. Signals were coded over a 20 min interval. Transmissions consisted of four-day periods, two to four times a month, spaced at every 4 hours. The data started to be collected in December 28 1995. The travel time data were obtained in near real time, and estimates of range-averaged temperature were obtained through stochastic inversion within a few days after the data were collected. The raw acoustic data from each receiver array consisted of time series of acoustic pressure at each of 40 hydrophones.

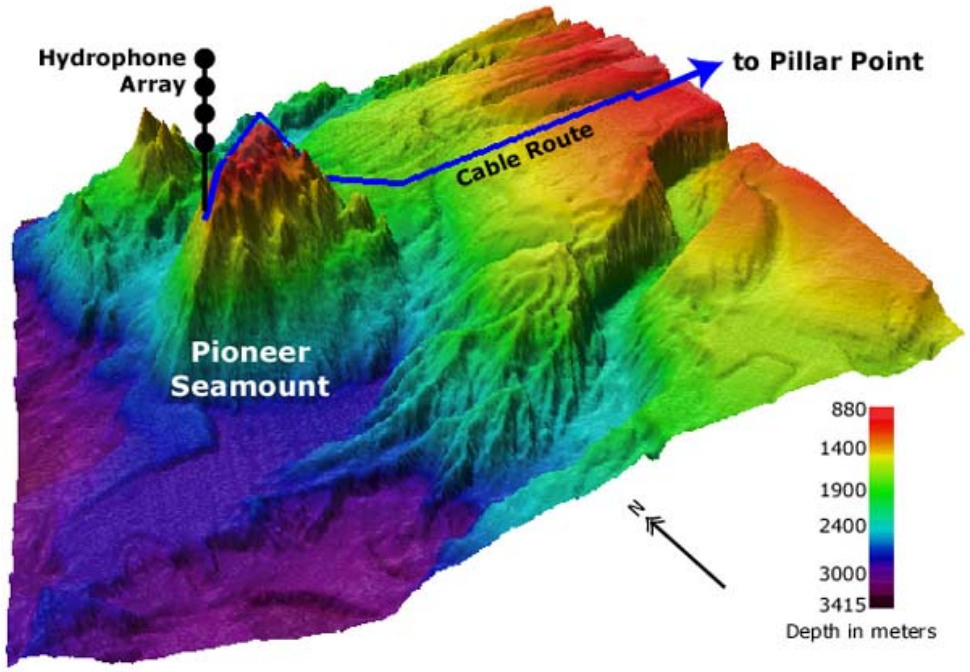

Figure 2.1: General overview of the receiving array at the Pioneer Seamount.

2.2.4 Small (coastal) scales

The Barents Sea Polar Front Tomography Experiment

In August 1992 the first coastal acoustic tomography test experiment was conducted over the steep northwestern slope of the Bear Island Through, about 100 km of Bear Island, during the Barents Sea Polar Front Tomography Experiment [14, 15] (see Fig.2.2). The purpose of the experiment was to characterize and understand the dynamics of the Barents Sea Polar Front (hereafter BSPF) using acoustic tomography coupled with traditional physical oceanographic techniques to map and study the oscillations of the BSPF. The field experiment was designed to demonstrate the feasibility of acoustic tomography in a shallow water environment, whit a bottom depth between 100 to 400 m. Two acoustic sources with a 400 Hz center frequency and a 100 Hz bandwidth, one near-bottom acoustic source with a 224 Hz center frequency and a 32 Hz bandwidth, and a vertical line array

with 16 hydrophones were used during the experiment. Characteristic ranges were around 35 km. The acoustic ray-tracing HARPO model was used to calculate stable eigenrays. Travel time perturbations were used in conjunction with a hybrid ray-mode inverse method to estimate the perturbations on sound speed. Inversion results allowed to map the BSPF with a horizontal resolution of 4 to 8 km and a vertical resolution of 30 to 80 m, which at the time of the experiment was considered to be the highest that could be achieved through acoustic techniques. Increasing the resolution in the horizontal direction was considered to be possible by increasing the number of modal arrivals.

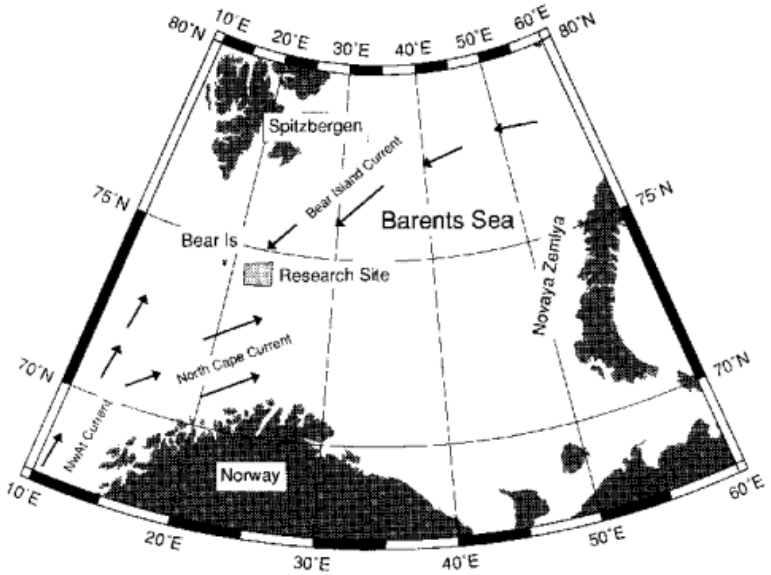

Figure 2.2: General overview of the experimental site during the Barents Sea Polar Front Tomography Experiment.

The INTIMATE'96 Experiment

The INTIMATE'96 sea trial, dedicated to the application of Ocean Acoustic Tomography for the monitoring of internal tides in coastal waters, took place during June of 1996 in Portuguese waters [16, 17]. Transmissions were developed using linear frequency modulated (LFM) signals, with a 550 Hz center frequency and a 250 Hz bandwidth, which was received on a vertical line array with 3 hydrophones located at 35, 105 and 115 m depth. Travel time perturbations were related to a basis of hydrostatic normal modes (hereafter HNMs) by parametrizing sound speed perturbations on a that basis [16]. Further, the amplitudes of HNMs were estimated through linear inversion. Inversion results indicate that under an accurate synchronization of the emitted and received signals the perturbation on sound speed can be accurately estimated in both range-independent and range-dependent approximations of acoustic propagation (see [17] and [18], respectively).

Chapter 3

Simulations

This chapter will introduce a general overview of the area contained in the Portuguese EEZ, the oceanographic data used for an environmental characterization of the area and the results of ray tracing acoustic simulations based on the oceanographic data.

3.1 The Portuguese EEZ

The Portuguese EEZ extends between mainland Portugal and the Açores and Madeira archipelagos, covering a rectangle of approximately 2,5 Mm × 2 Mm, with a corresponding area of 5 Mm^2, as shown in Fig.3.1. The extension of the EEZ determines the boundaries and bathymetry of the area which is intended to be monitored through acoustic tomography.

3.2 Oceanographic data and bathymetry

Temperature and salinity data from NODC datasets for the interior of the Portuguese EEZ were roughly averaged over one year in order to calculate sound speed distributions along three transects (hereafter T1, T2 and T3), crossing the area of interest as shown in Fig.3.2. Additionally, the general bathymetry of the area (also shown in Fig.3.2) was determined using satellite ETOPO5 data, and indicates that the main variations of bottom depth take place near the continental slope of mainland Portugal and the location of both Açores and Madeira archipelagos, with sudden variations of bottom depth of the order of 5 km.

Each transect covers a surface layer lasting between 10 and 390 m and contains a total of approximately 40 local averages of temperature and salinity, which were converted to sound speed using Mackenzie's formula [19] (see Fig.3.3). The bathymetry along each transect was calculated using ETOPO5 satellite data and is shown in Fig.3.4.

The independency of environmental conditions along each transect is well reflected on the corresponding range-dependent structure of sound speed. Much of that independency can be estimated through the Singular Value Decomposition [20] (hereafter SVD) of the data matrix containing the samples of each transect, and further plotting of the singular

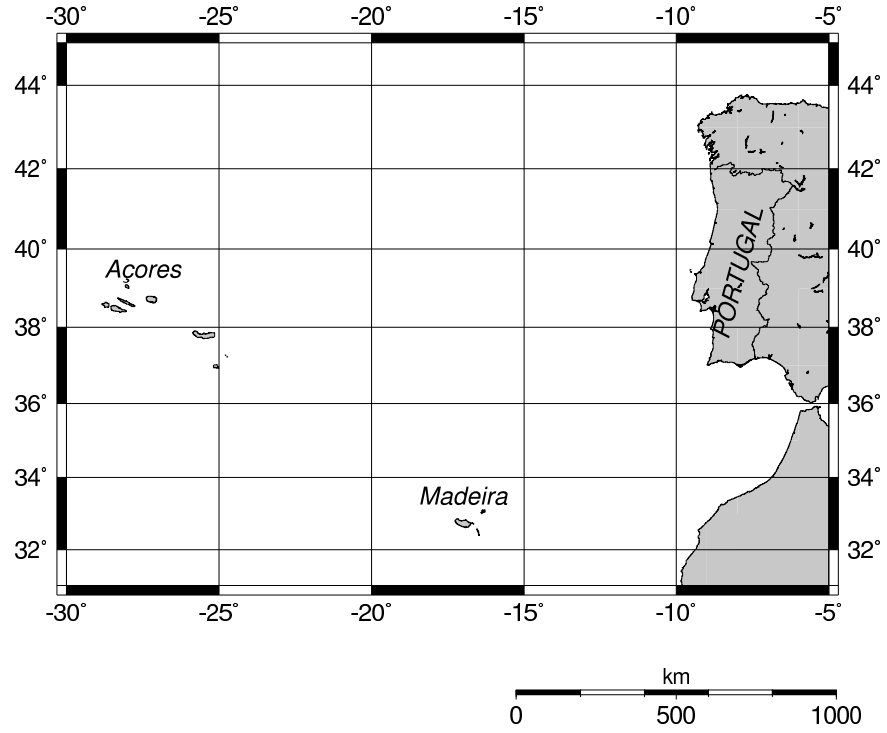

Figure 3.1: General overview of the Portuguese EEZ.

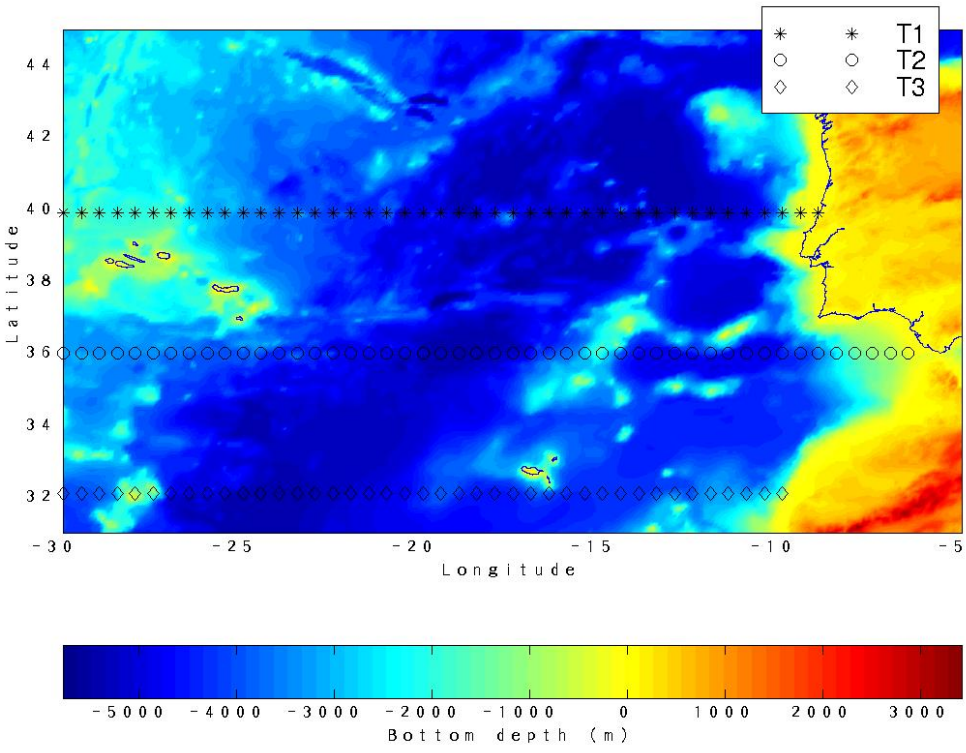

Figure 3.2: Portuguese EEZ bathymetry and selected transects T1, T2 and T3.

(a)

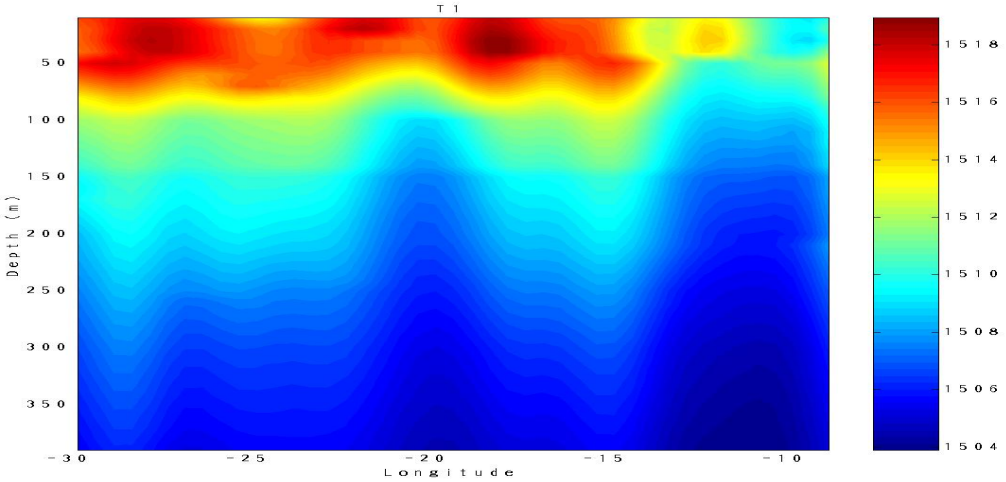

(b)

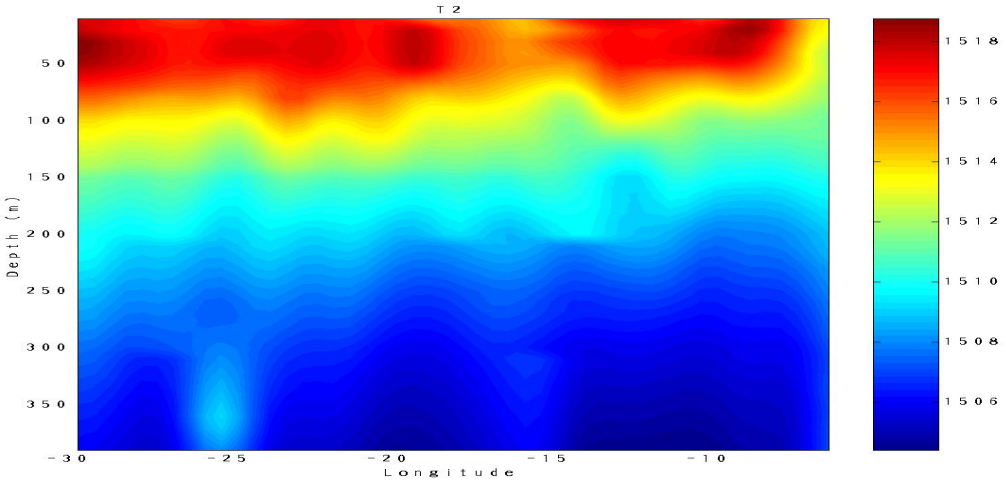

(c)

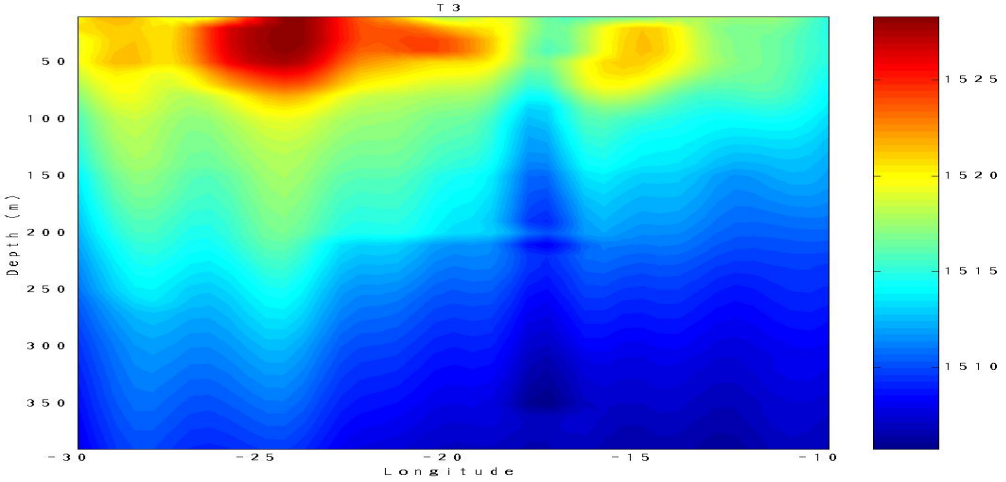

Figure 3.3: Sound speed distributions: (a) T1; (b) T2; (c) T3.

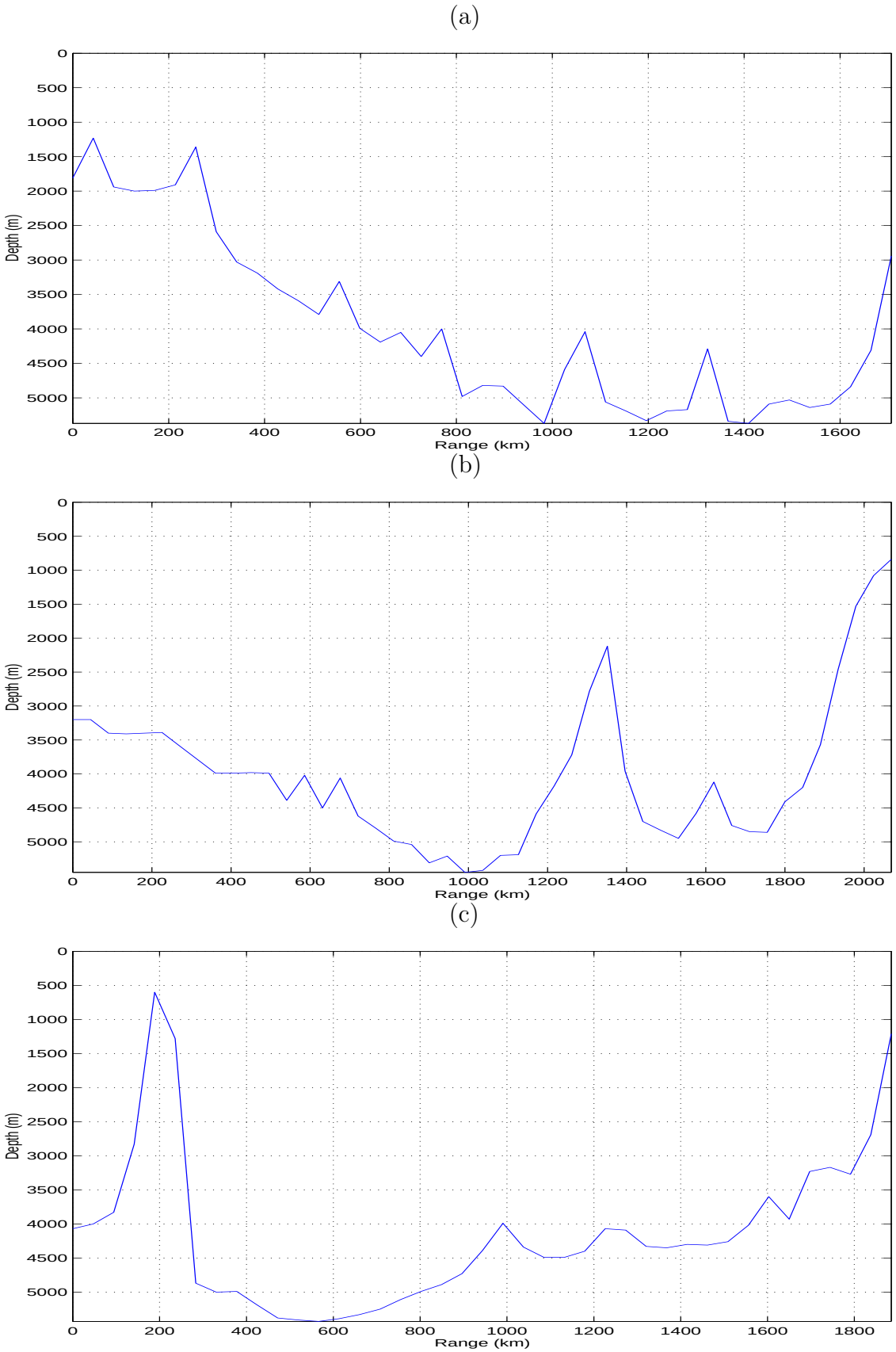

Figure 3.4: Transects bathymetry: (a) T1; (b) T2; (c) T3. In all cases range increases towards mainland Portugal, with range "0" corresponding to longitude -30°.

values of the diagonal matrix obtained from the SVD. The distributions of eigenvalues can be seen in Fig.3.5, and indicate that practically all energy is contained in the first 15 eigenvalues, thus indicating a number of fifteen independent eigenfunctions for each transect. However, among those fifteen eigenfunctions the first four already count for practically 80% of the total energy, implying that a reduced number of basis eigenfunctions can be used efficiently to monitorize a significant part of the environmental dynamics.

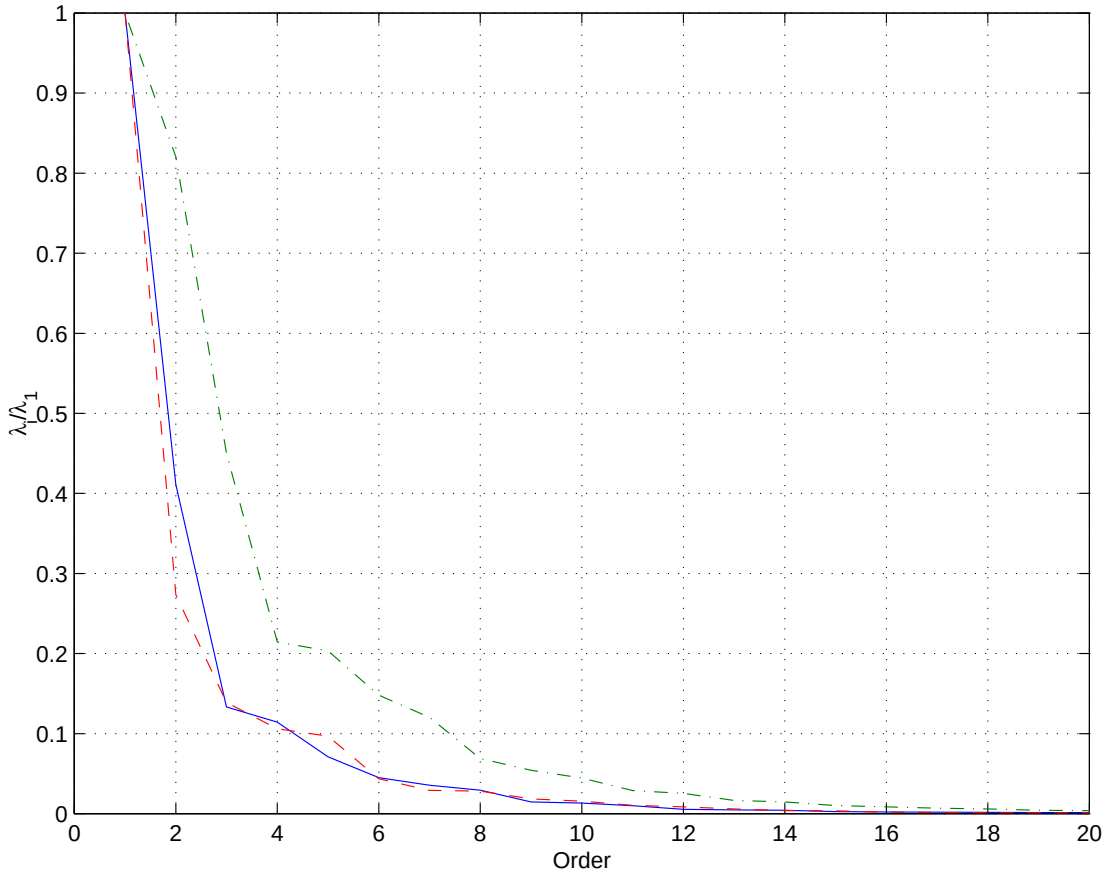

Figure 3.5: Normalized distribution of eigenvalues for T1 (continuous line), T2 (dot-dashed line) and T3 (dashed line).

3.3 Range independent simulations

Sound propagation at basin scales is strongly characterized by the variations of sound speed along the propagation track, horizontal refraction of the sound field, and significant variations of bathymetry [11]. For the particular scales of the Portuguese EEZ neglecting horizontal refraction can be considered as a realistic approximation, whereas neglecting bathymetry and sound speed variations may not be. Nevertheless, a range independent model of propagation can be a good starting point in order to estimate the expected temporal separation of acoustic arrivals, eigenray stability, and the robustness of the inversion methods to be applied to the acoustic data.

3.3.1 Sound speed profile

T1 was considered to be the "smoothest" of the transects to develop the simulations. The corresponding transect data was used to calculate the mean sound speed profile $c_0(z)$, which was extrapolated up to the maximum transect depth, D, to a Munk profile $c_M(z)$ [21]:

$$c_M(z) = c_a \left[1 + \epsilon \left(\eta(z) + e^{-\eta(z)-1}\right)\right] \ , \tag{3.1}$$

where

$$\eta(z) = 2\frac{z - z_a}{B} \ , \tag{3.2}$$

and $B = 1,3$ km, $\epsilon = 7,4 \times 10^{-3}$. The "axial" parameters c_a and z_a were calculated numerically from the conditions

$$c_0(z_1) = c_M(z_1) \quad \text{and} \quad \frac{dc_0}{dz} = \frac{dc_M}{dz} \quad \text{at} \quad z = z_1 \ . \tag{3.3}$$

Both $c_0(z)$ and $c_M(z)$ can be seen in Fig.3.6 . The extrapolated profile indicates a depth of the channel axis, z_a, located near 700 m, which induces the formation of a SOFAR channel which extends from the surface until 2000 m depth. It is important to remark that the values of sound speed of the extrapolated profile contrast significantly with the profiles described in the known literature (see, for instance, the deep water profile for the North Pacific described in [21]) which is believed to be due to significant differences in surface warming at different latitudes.

The range-dependent structure of sound speed along T1, $c(z, r)$, was obtained –formally– extrapolating each profile of the original data presented in Fig.3.3(a) (as previously described for the mean sound speed), along the bathymetry shown in Fig.3.4(a). That structure was found to be more or less homogeneous above and below the channel axis, with a significant variation of environmental conditions along the axis itself (see Fig.3.7(a)). In contrast with that distribution the expected perturbation of sound speed, $\delta c(z, r)$ (see Fig.3.7(b)), was found to be extremely variable, exhibiting an interesting intrusion of warm waters between 1500 and 3000 m, from the side of mainland Portugal. Taking into account the lack of knowledge regarding such kind of phenomena the observed feature was not considered to be as representing real conditions.

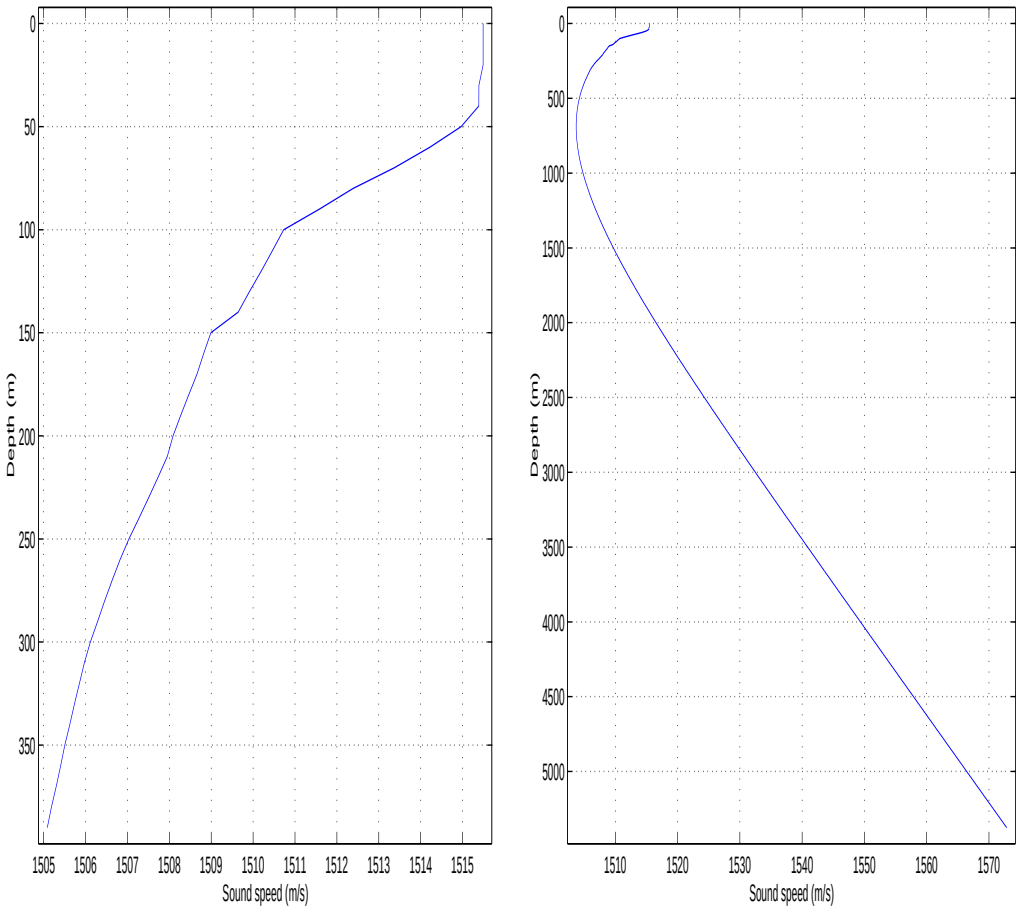

Figure 3.6: Mean sound speed profile $c_0(z)$ for T1: (a) mean average of available data; (b) corresponding Munk extrapolation up to the maximum depth.

(a)

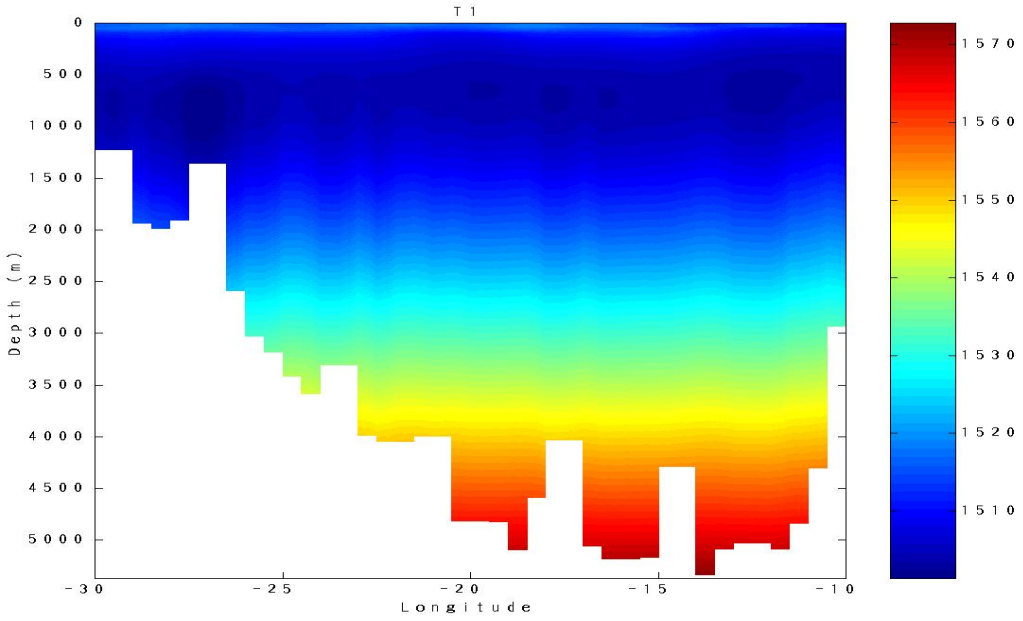

(b)

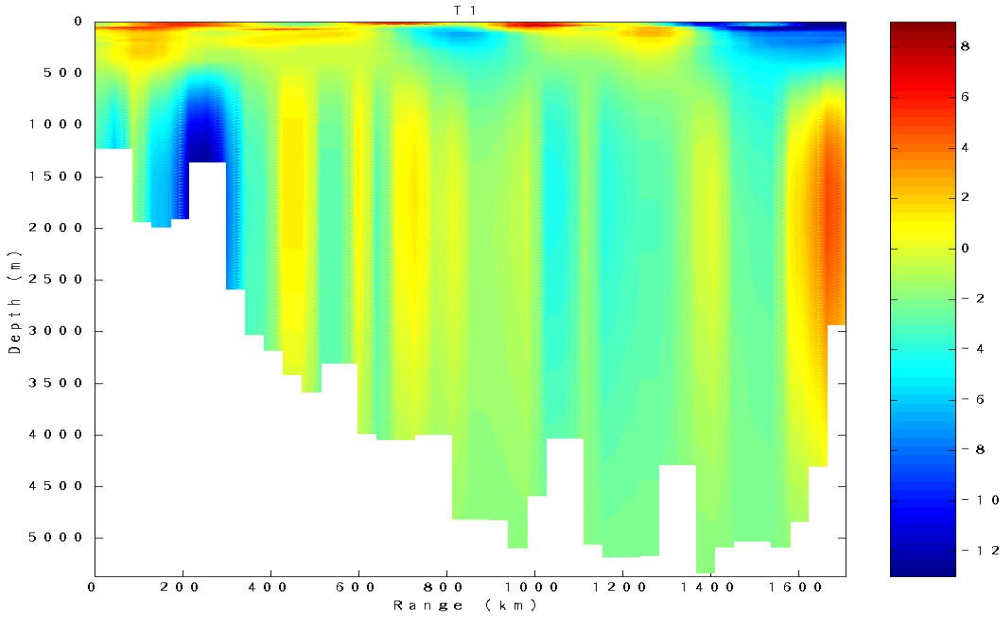

Figure 3.7: Extrapolated range-dependent sound speed distribution $c(z, r)$ along T1 (case (a)) and expected sound speed perturbation $\delta c(z, r)$ (case (b)).

3.3.2 Source positioning

A fundamental criterion for the positioning of the acoustic source is to ensure the propagation of refracted eigenrays, spanning the watercolumn at turning depths as different as possible. This situation only takes place when the distribution of launching angles is simmetric above and below source depth, which –according to Snell's law– is only possible by positioning the source at the depth of the SOFAR channel axis. Thus, during the development of the simulations it was considered that the acoustic source was towed at z_a.

3.3.3 Receiver positioning

The number of eigenrays arriving at a particular depth depends non-linearly on receiver range and sound speed. However, at the receiver position it should be expected not only that a significant number of eigenrays will arrive, but it should be expected also that those eigenrays will have refracting depths as different as possible. Once the acoustic source has been towed at a particular depth a straightforward ray tracing (not involving eigenray calculations) can provide some preliminary information regarding that issue. Taking into account the discussion presented in the previous section let us consider that the acoustic source is located at z_a, and let us develop some ray tracing calculations using the extrapolated profile shown in Fig.3.6(b) for a range $R = 50$ km, in order to determine the depth at R of the rays launched in the interval $\theta \in [-20°, 20°]$ (represented hereafter as $\zeta(\theta, R)$). The results, shown in Fig.3.8(a), indicate a symmetric distribution of $\zeta(\theta, R)$ between -14° and 14°. Furthermore, the distribution suggests that positioning the receivers between 2500 and 4500 m will allow to account for between 1 and 5 eigenrays, in contrast with the 9 eigenrays that can be expected by positioning the receivers between 0 and 1500 m. In this sense, the geometry of transmissions with $R = 50$ km suggests to use the array spanning the upper part of the watercolumn, above and below the channel axis, with the highest hydrophone near to the surface and the lowest hydrophone near 1500 m. Increasing the range between the source and the system of receivers do not seem affect that consideration: in fact, repeating the calculations for $R = 1000$ km (Fig.3.8(b)) it can be expected a significant increase of the number of eigenrays near the channel axis, and a "clustering" of many eigenrays between 2000 and 4000 m depth. However, that clustering takes place within a reduced interval of θ, for wide and close angles, suggesting that the corresponding eigenrays will be refracted at close depths (or perhaps will be reflected on surface and/or bottom), reducing significantly the independency of information that those eigenrays gather for inversion. On the other hand, as in the case with $R = 50$ km, the expected distribution of eigenrays for $R = 1000$ km seems to be periodic-like near the channel axis (for instance near 1000 m), with an uniform distribution of launching angles between -15° and 15°.

3.3.4 Ray tracing

The starting point for the development of ray tracing consisted in selecting a "perturbed" sound speed profile $c(z)$. For the sake of consistency with the data available for T1 the deepest profile of the dataset shown in Fig.3.7(a), near longitude -14°, was selected to be representative of $c(z)$ (see Fig.3.9(a)). Although the corresponding perturbation of sound speed, shown in Fig.3.9(b), exhibits a narrow channel near the surface the overall behaviour below 200 m seemed to be physically realistic. Bathymetry variations were

not taken into account, and following the discussion presented in sections 3.3.2 and 3.3.3 the ray tracing was developed considering the acoustic source located at z_a and a single receiver located at 1000 m. Two sets of arrivals were generated: the first for the mean profile shown in Fig.3.6(b)), and the second for the perturbed profile shown in Fig.3.9(a)). A total of 47 RSR stable eigenrays were found after calculations (some of them can be seen in Fig.3.10(a)). The fact that most of stable eigenrays exhibit many ray loops within the waveguide should not be surprising: in fact, eigenrays with a few loops will appear only when the rays are launched at small angles, but those rays, according to Fig.3.8, are not able to achieve depths below 1000 m. Calculated arrivals spread over a transmission window of 30 s, a mean temporal separation of 0.6 s and with most of the arrivals clustered in the initial 10 s.

3.3.5 Sound speed parameterization

Before describing the general method of inversion it is important to notice that the perturbation on sound speed was parameterized using a set of Hydrostatic Normal Modes (hereafter HNMs)

$$\delta c(z) = c(z) - c_M(z) = \sum_{m=1}^{M} \alpha_m \Psi_m(z) \ , \tag{3.4}$$

where the eigenfunctions $\Psi_m(z)$ were calculated by solving a standard Sturm-Liouville problem of the following form:

$$\frac{d^2\Psi_m}{dz^2} + \frac{N^2}{c_m^2}\Psi_m = 0 \quad \text{and} \quad \Psi_m(0) = \Psi_m(D) = 0 \ . \tag{3.5}$$

The buoyancy frequency $N(z)$ was taken as

$$N(z) = N_0 e^{(-z/B)} \ , \tag{3.6}$$

where $N_0 = 2.8$ cycles/hour [21, 22]. The existence of an unique set of modal amplitudes, α_m, was guaranteed by the orthogonality of the HNMs. It is important to remark that the choice of the parameter N_0 does not reflect any local characteristic of T1. In this sense it is expected that the usage of the HNMs calculated with the given set of parameters will certainly introduce a level of mismatch, which is difficult to estimate *apriori*.

3.3.6 Inversion results

Linear inversion and parameterization with four HNMs were combined to develop the inversion. Briefly, given the relationship [20][17]

$$\boldsymbol{\Delta\tau} = \mathbf{S}\boldsymbol{\alpha} + \mathbf{n} \ , \tag{3.7}$$

where the vector $\boldsymbol{\Delta\tau}$ contains a "collection" of travel time delays, $\mathbf{S}$ corresponds to the kernel matrix (calculated from eigenrays and HNMs), $\boldsymbol{\alpha}$ is a vector whose components are the modal amplitudes α_m of Eq.(3.4), and $\mathbf{n}$ represents the contribution of all sources of noise, the estimated least-squares solution can be written as [1]

$$\boldsymbol{\alpha}^{\#} = \left(\mathbf{S}'\mathbf{S}\right)^{-1}\mathbf{S}'\boldsymbol{\Delta\tau} \ . \tag{3.8}$$

The estimate of δc can be seen in Fig.3.11. Not surprisingly the narrow channel is not estimated but in general the estimated solution accurately follows the phase and the amplitude of the expected perturbation.

3.4 Range dependent simulations

The range-dependent ray-tracing model `ray` was used to calculate eigenrays and travel times for the mean sound speed profile (see Fig.3.6(b)) and the extrapolated distribution of sound speed shown in Fig.3.7(a). The main objective of the simulation was to introduce a range-dependent parameterization of perturbation on sound speed:

$$\delta c(z,r) = c(z,r) - c_m(z) = \sum_{m=1}^{M} \alpha_m R_m(r) \Psi_m(z) \ , \tag{3.9}$$

on the orthogonal bases $R_m(r)$ and $\Psi_m(z)$[1]. A preliminary (and numerically intensive) attempt to estimate the modal amplitudes using a Fourier synthesis failed due to the large number of coefficients that were needed to ensure the accuracy of estimation. In fact, the main conclusion of the range-dependent estimation is that although any choice of $R_m(r)$ is mathematically allowed it is desirable to use a basis which guarantees the convergence of the estimate with a few eigenfunctions. Thus, the choice of an appropriate basis is a fundamental issue whose discussion goes beyond the original purpose of this report. An additional problem found during the estimation consisted in the difficulties in finding stable eigenrays. In fact, as discussed in [11] the strategy of using a range independent profile to determine the eigenrays can be extremely ineffective due to the importance of refraction effects as the position of axis channel changes with range.

[1] A parameterization of the form

$$\delta c(z,r) = c(z,r) - c_m(z) = \sum_{m=1}^{M} \alpha \Psi_m(z,r) \ ,$$

would be more desirable, although it is not clear which eigenfunctions $\Psi_m(z,r)$ are be "available" for this purpose.

(a)

(b)

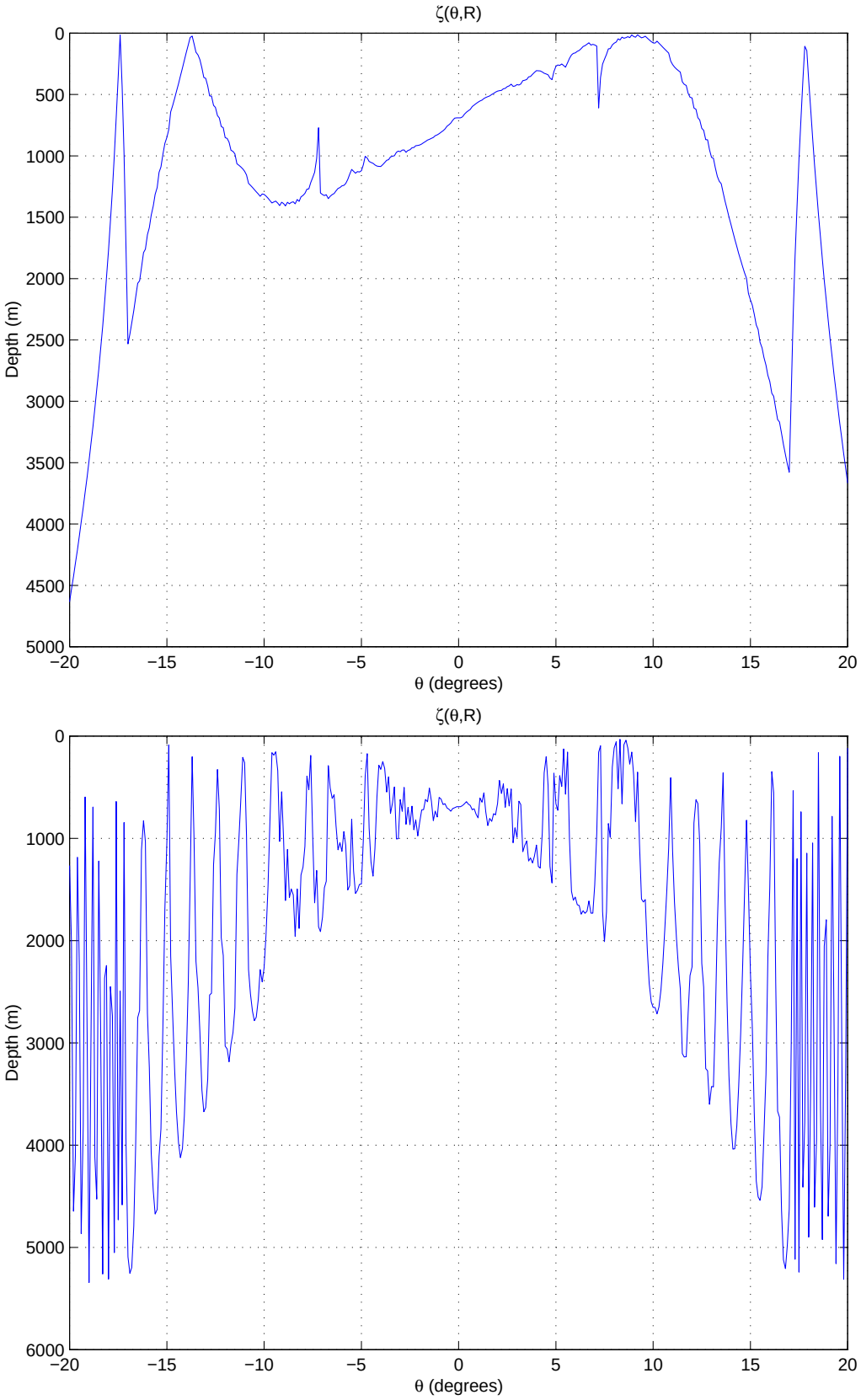

Figure 3.8: Ray depth distribution $\zeta(\theta, R)$ for $\theta \in [-20°, 20°]$, at $R = 50$ km (case (a)) and $R = 1000$ km (case (b)).

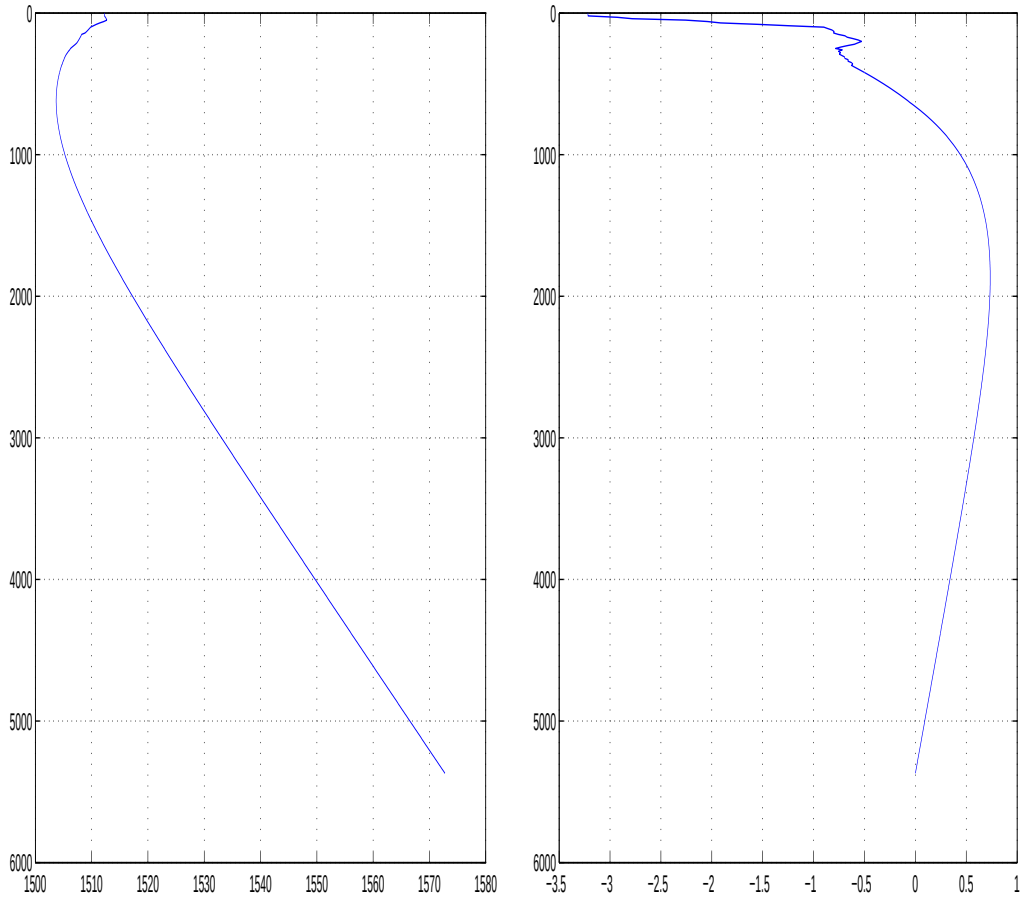

(a) (b)

Figure 3.9: Perturbed sound speed profile $c(z)$ for T1: (a) Munk extrapolation at the deepest site of T1; (b) corresponding sound speed perturbation $\delta c(z) = c(z) - c_0(z)$.

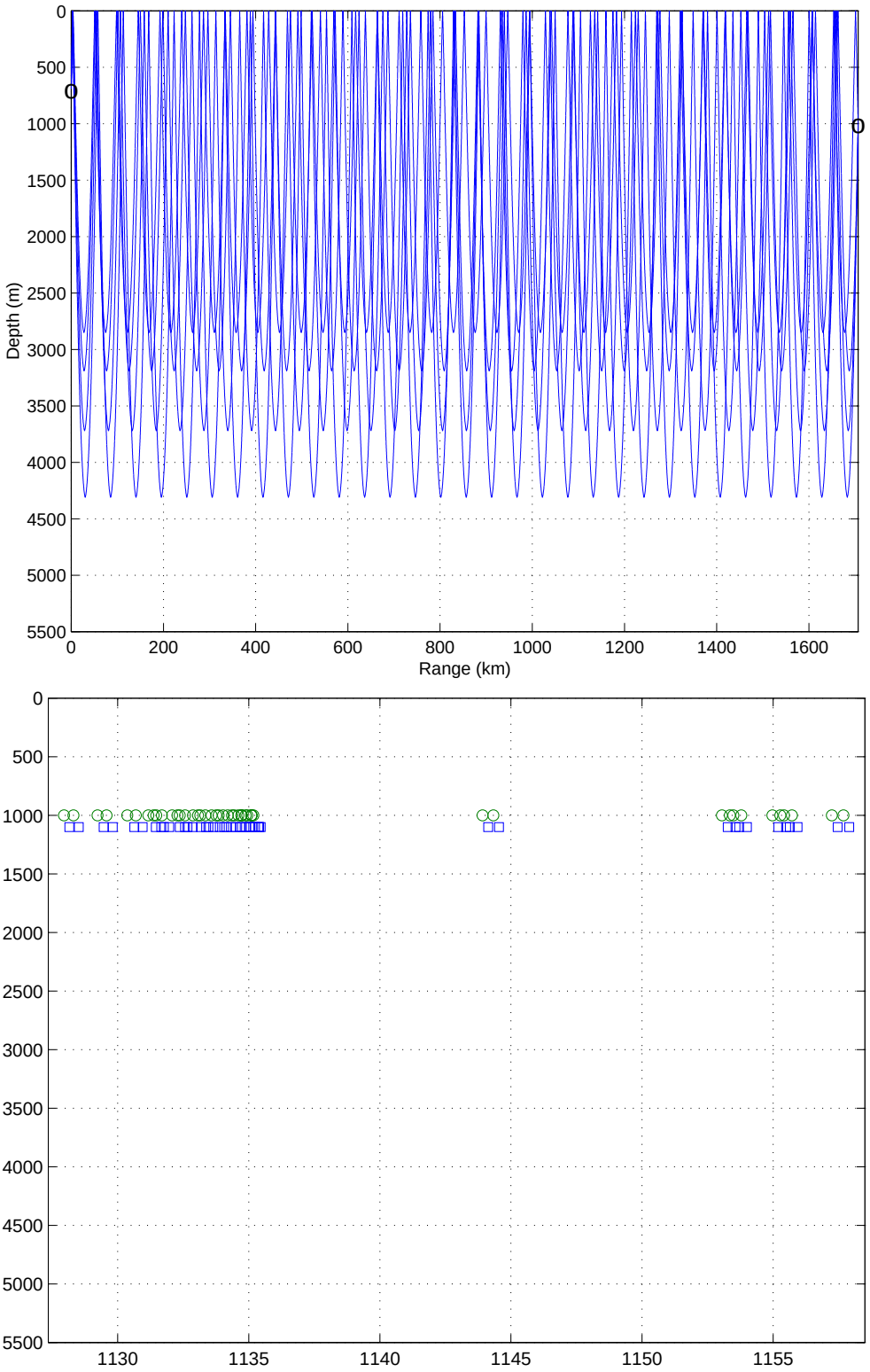

Figure 3.10: (a) Some stable eigenrays, the circles indicate the position of the source and the receiver; (b) temporal dispersion of arrivals.

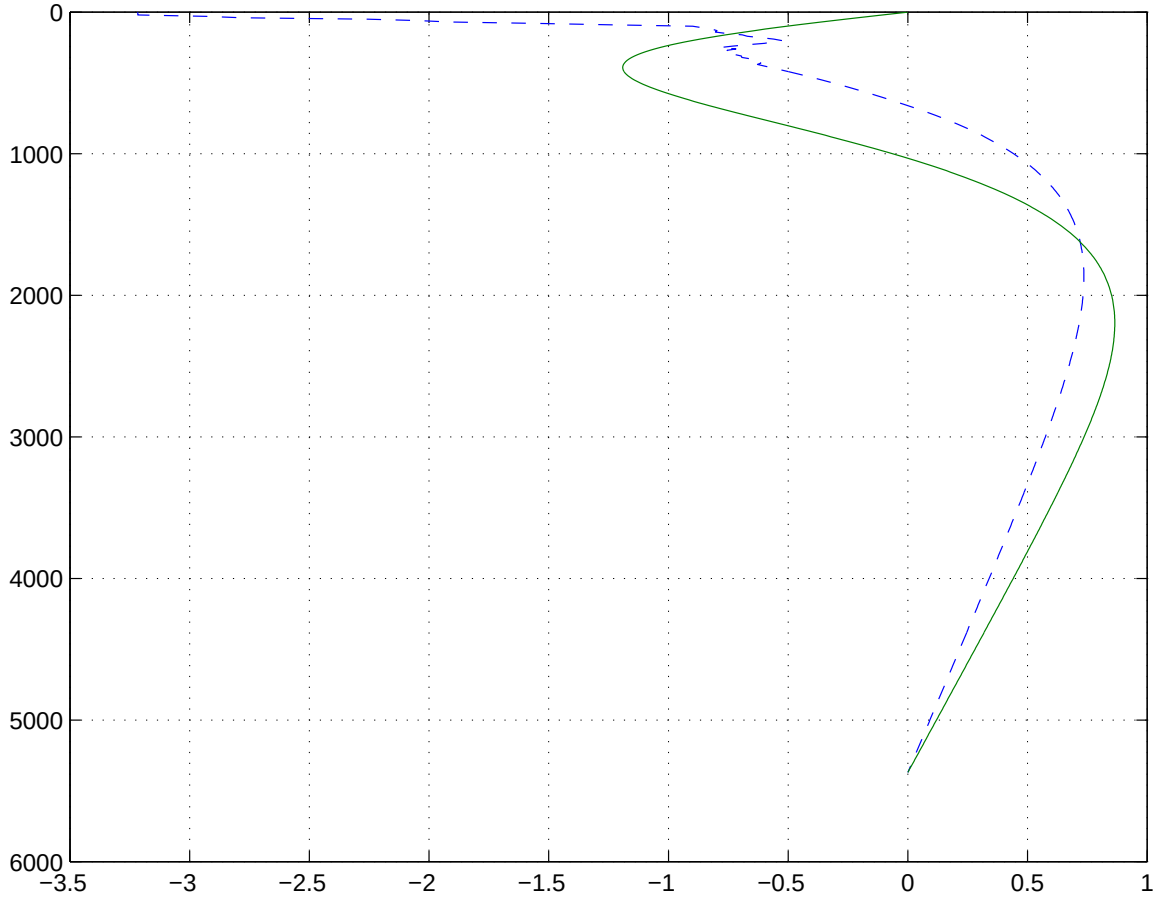

Figure 3.11: Expected perturbation of sound speed $\delta c(z)$ (dashed line) and estimate (continuous line).

Chapter 4

Conclusions

The main conclusions obtained during the discussion of the bibliographic review and long range simulations can be summarized as follows:

- Well known experiments and existent literature confirm that acoustic signals can be used as an efficient tool to infer the environmental variations of large ocean masses, with the associated technical and scientific impacts (and benefits) that the corresponding application of acoustic signals imply.
- A natural choice for an effective and secure support of acoustic transmissions at long ranges corresponds to the usage of signal modulation based on binary m-sequences, which had been shown to ensure the required resolution of travel times, and compactness of signal energy without harming marine life.
- Preliminary simulations based on a hypothetical range independent environment of acoustic propagation allowed to estimate the expected temporal spread of received arrivals, thus providing some preliminary constrains for the choice of the signal bandwidth.
- For the range independent scenario of acoustic propagation the damped least squares solution, associated with the construction of the L-shape curve, ensured a robust and accurate method of estimating the perturbation of sound speed.
- Selecting refracted eigenrays (and disregarding eigenrays reflected on both surface and/or bottom) does not allow to account for the effects of bottom bathymetry. However, one can expect that accounting for reflected eigenrays will turn the identification of acoustic arrivals into a difficult task, independently of using simulated or real acoustic data.
- Physical and computational models are strongly needed in order to properly analyze the effects of bottom bathymetry, variations of sound speed in range and depth, and also to determine a reliable basis of eigenfunctions for range dependent inversion.

Bibliography

[1] Munk W., Worcester P., and Wunsch C. *Ocean Acoustic Tomography*. Cambridge Monographs on Mechanics, Cambridge, University Press, 1995.

[2] Cornuelle B.D. et al. Tomographic Maps of the Ocean Mesoscale. Part 1: Pure Acoustics. *J. of Physical Oceanography*, 15:133–152, February 1985.

[3] Chiu C-S. and Desaubies Y. A Planetary Wave Analysis Using the Acoustic and Conventional Arrays in the 1981 Ocean Tomography Experiment. *Journal of Physical Oceanography*, 17:1270–1287, August 1987.

[4] Tolstoy A., Diachok O., and Frazer L.N. Acoustic tomography via matched field processing. *J. Acoust. Soc. America*, 89(3):1119–1127, March 1991.

[5] Karangelen C. and Diachok O. Experimental demonstration of sound-speed inversion with matched-field processing. *J. Acoust. Soc. America*, 93(5):2649–2655, May 1993.

[6] Lawson L.M. and Palmer D.R. Acoustic ray-path fluctuations induces by El Niño. *J. Acoust. Soc. America*, pages 1343–1345, May 1984.

[7] Shang E.C. and Wang Y.Y. On the possibility of monitoring El Niño using modal ocean acoustic tomography. *J. Acoust. Soc. America*, 91(1):136–140, January 1992.

[8] Shang E.C. Ocean acoustic tomography based on adiabatic mode theory. *J. Acoust. Soc. America*, 85(4):1531–1537, April 1989.

[9] Porter M. *The KRAKEN normal mode program*. SACLANT UNDERSEA RESEARCH (memorandum), San Bartolomeo, Italy, 1991.

[10] Spindel R.C. *Adaptive Methods in Underwater Acoustics*. Reidel Publishing Company, 1985.

[11] Dushaw et al. The Acoustic Thermometry of Ocean Climate (ATOC) Project: Towards depth-averaged temperature maps of the North Pacific Ocean. In *Proceedings of the International Symposium on Acoustic Tomography and Thermometry*, Tokyo, Japan, 8-9 February 1999.

[12] Dushaw B.D. et al. Multi-megameter range acoustic data obtained by bottom-mounted hydrophone arrays for measurement of ocean temperature. *IEEE J.Ocean. Engin.*, 24(2):202–214, April 1999.

[13] Dushaw B.D. Inversion of Multimegameter-Range Acoustic Data for Ocean Temperature. *IEEE J.Ocean. Engin.*, 24(2):215–223, April 1999.

[14] Ching-Sang Chiu, Miller J.H., and Lynch J.F. Inverse Techniques for Coastal Acoustic Tomography. In D. Lee and H. Schultz, editors, *Theoretical and Computational Acoustics*, pages 917–931, World Scientific, Singapore, 1994.

[15] Ching-Sang Chiu, Miller J.H., Denner W., and Lynch J.F. Forward modeling of the Barents sea tomography vertical line array data and inversion highlights. In O. Diaschok et al, editor, *Full Field Inversion Methods in Ocean and Seismo-Acoustics*, pages 237–242, Kluwer Academic Publishers, Netherlands, 1995.

[16] Rodríguez O.C., Jesus S., Stéphan Y., Démoulin X., Porter M., and Coelho E. Internal tide acoustic tomography: reliability of the normal modes expansion as a possible basis for solving the inverse problem. In *Proc. of the 4th. European Conference on Underwater Acoustics*, pages 587–592, Rome, Italy, 21-25 September 1998.

[17] Rodríguez O. C. *Application of Ocean Acoustic Tomography to the estimation of internal tides on the continental platform.* PhD. Thesis, Faculdade de Ciências e Tecnologia–Universidade do Algarve (FCT-UALG), Faro, Portugal (available in ftp://ftp.ualg.pt/users/siplab/doc), December, 2000.

[18] Rodríguez O.C. and Jesus S. M. Range-dependent Regularization of Travel Time Tomography based on Theoretical Modes. In *Proc. of the 6th. European Conference on Underwater Acoustics*, pages 515–520, Gdansk, Poland, 24-27 June 2002.

[19] Mackenzie K.V. Nine-term equation for the sound speed in the oceans. *J. Acoust. Soc. America*, 70(3):807–812, 1981.

[20] Menke W. *Geophysical Data Analysis: Discrete Inverse Theory.* Academic Press, Inc, San Diego, California, 1989.

[21] Buckingham M.J. Ocean acoustic propagation models. Technical Report EUR 13810, Comission of the European Communities, 1991.

[22] Athanassoulis G.A. and Skarsoulis E.K. Arrival-time perturbations of broadband tomographic signals due to sound-speed disturbances. A wave-theoretic approach. *J. Acoust. Soc. America*, 97(6):3075–3588, June 1995.

Appendix I

M-sequences

I.1 Preliminary definitions

1. The *modulus* operation between two integers x and y, denoted as $y \,(\mathrm{mod}\ x)$, corresponds to the remainder of the division of y by x:

$$r = y \,(\mathrm{mod}\ x) \Leftrightarrow r = y - mx \ , \tag{A.I.1}$$

with m being the largest integer that verifies $y - mx > 0$.

2. The *order* of a polynomial $h(x)$, for which $h(0) \neq 0$, is the smallest integer n for which $h(x)$ divides x^n+1. For instance, the order of the polynomial $h(x) = x^2+x+1$ is $n = 3$ since $x^3 + 1/h(x) = (x + 1)$.

3. A polynomial $h(x)$ of the form

$$h(x) = h_0 x^r + h_1 x^{r-1} + h_2 x^{r-2} + \ldots + h_{r-1} x + h_r \ , \tag{A.I.2}$$

where $h_0 = h_r = 1$ and $h_i \in 0, 1$, is said to be *primitive* if $h(x)$ can not be factored into non-trivial polynomials, and its order n is an odd integer: $n = 2^k - 1, k \in 1, 2, 3, ...$ For instance, the polynomial $h(x) = x^2 + x + 1$ is a primitive polynomial since its order is $n = 3$ and $h(x)$ can not be factored into non-trivial polynomials. An extensive table of primitive polynomials can be found in the Appendix II.

4. A sequence of integers $\{c_n\}$ is said to be a (binary) m-sequence of degree r if $\{c_n\}$ satisfies the linear recurrence relation:

$$c_n = \sum_{i=1}^{r} h_i c_{n-i} \,(\mathrm{mod}\ 2) \ , \tag{A.I.3}$$

with $n = r+1, r+2, \ldots, 2^r - 1$, and h_i being the coefficients of the primitive polynomial $h(x)$ of degree r[1]. In order to generate a binary m-sequence the initialization coefficients c_0, c_1, ..., and c_r should be specified (see section I.2).

[1]Binary m sequences are also called as maximal length, shift register or pseudorandom sequences or also pseudorandom noise.

Properties of m-sequences:

- The m-sequence has a period equal to $2^r - 1$.
- There are exactly $2^r - 1$ (nonzero) sequences generated by $h(x)$, which are cyclic shifts of each other.
- The sum (mod 2) of two m-sequences is another m-sequence generated by the same $h(x)$.
- The number of ones in each period corresponds to 2^{r-1}, while the number of zeros corresponds to $2^{r-1} - 1$.

I.2 Coefficients of m-sequences

In general the initialization coefficients are taken as $c_0 = 1$ and c_i $(i = 1, \ldots, r)$ being any possible combination of ones and zeros of length r, but not all zeros. The choice of initialization determines the location at which the periodicity of the m-sequence begins but it does no alter the sequence itself. In order to clarify those statements let us calculate the coefficients of the m-sequence of degree $n = 7$. The corresponding primitive polynomial of degree $r = 3$ corresponds to

$$h(x) = x^3 + x + 1 \ ,$$

with coefficients $[h_0 \ h_1 \ h_2 \ h_3] = [1 \ 0 \ 1 \ 1]$. Let us take the initialization coefficients as

$$[c_3 \ c_2 \ c_1 \ c_0]_1 = [0 \ 0 \ 1 \ 1] \ .$$

Then, applying the definition given by Eq.(A.I.3) one gets:

$$c_4 = h_1 c_3 + h_2 c_2 + h_3 c_1 \,(\text{mod } 2) = 1 \ ,$$

$$c_5 = h_1 c_4 + h_2 c_3 + h_3 c_2 \,(\text{mod } 2) = 0 \ ,$$

$$c_6 = h_1 c_5 + h_2 c_4 + h_3 c_3 \,(\text{mod } 2) = 1 \ ,$$

and

$$c_7 = h_1 c_6 + h_2 c_5 + h_3 c_4 \,(\text{mod } 2) = 1 \ .$$

In this way the coefficients c_i of the m-sequence will correspond to

$$[c_7 \ c_6 \ \ldots \ c_0]_1 = [1 \ 1 \ 0 \ 1 \ 0 \ 0 \ 1 \ 1] \ .$$

Now, taking the initialization coefficients as

$$[c_3 \ c_2 \ c_1 \ c_0]_2 = [h_3 \ h_2 \ h_1 \ 1] = [1 \ 1 \ 0 \ 1] \ .$$

allows to obtain the m-sequence

$$[c_7 \ c_6 \ \ldots \ c_0]_2 = [1 \ 0 \ 0 \ 1 \ 1 \ 1 \ 0 \ 1] \ ,$$

which –excluding the coefficient c_0– is a shifted version of the first m-sequence.

Remarks:

1. Binary m-sequences are often represented in octal representation. Thus, the sequence $[\ldots]_1$ corresponds to 323_8, while the sequence $[\ldots]_2$ corresponds to 235_8.

2. For a fixed r the number N of primitive polynomials is given by $N = \phi(2^r - 1)/r$, where ϕ corresponds to the Euler "totient" function. Since $N \geq 1$ the choice of a primitive polynomial is not unique and different primitive polynomials of the same order will provide different m-sequences. For instance, there are two different primitive polynomials of order $r = 3$, which correspond to

$$h(x) = x^3 + x + 1 \qquad \text{and} \qquad h(x) = x^3 + x^2 + 1 \ .$$

   Thus, for the initialization coefficients

$$[c_3\ c_2\ c_1\ c_0]_1 = [0\ 0\ 1\ 1]$$

   selecting the second polynom instead of the first one will provide the following sequence:

$$[c_7, c_6, \ldots, c_0]_I = [0\ 1\ 1\ 1\ 0\ 0\ 1\ 1] \ ,$$

   which is different from $[\ldots]_1$. Further, the initialization coefficients

$$[c_3\ c_2\ c_1\ c_0]_2 = [1\ 0\ 0\ 1]$$

   provides

$$[c_7, c_6, \ldots, c_0]_{II} = [1\ 0\ 1\ 1\ 1\ 0\ 0\ 1] \ ,$$

   which confirms the shift property of the sequence.

3. The primitive polynomial can be denoted also as

$$h(x) = h_r x^r + h_{r-1} x^{r-1} + h_{r-2} x^{r-2} + \ldots + h_1 x + h_0 \ . \tag{A.I.4}$$

   Thus, for a common set of initialization coefficients c_0, c_1, ..., c_r, the binary m-sequences generated using the definition Eq.(A.I.2) and the definition Eq.(A.I.4) will coincide on the the first r coefficients, but will contain the remaining zeros and ones at different positions. For instance, for the primitive polynomial $h(x) = x^3 + x^2 + 1$ the initialization coefficients $[c_3\ c_2\ c_1\ c_0] = [0\ 0\ 1\ 1]$, together with the definition Eq.(A.I.4), provide the m-sequence

$$[c_7, c_6, \ldots, c_0] = [1\ 1\ 0\ 1\ 0\ 0\ 1\ 1] \ .$$

   Curiously, the primitive polynomial $h(x) = x^2 + x + 1$ provides the same m-sequences independently of which definition is used.

I.3 Signal modulation based on m-sequences

Let us consider a signal $g(t)$, constructed by repeating a prototype signal $p(t)$, L times, with time step T and modulated by a sequence of coefficients $[m_{L-1}, m_{L-2}, \ldots, m_0]$:

$$g(t) = \sum_{l=0}^{L-1} m_l p(t - lT) \ , \tag{A.I.5}$$

where $m_l = \exp(ic_l\theta_0)$, and the coefficients $[c_{L-1}, c_{L-2}, \ldots, c_0]$ corresponding to a binary m-sequence but replacing the ones in the sequence with the value -1 and the zeros with the value +1. The prototype signal is chosen to be the periodic repetition of a single digit (i.e., a periodic pulse train with period LT); $g(t)$ is then a continuing periodic signal with period LT. The period LT must be chosen to be longer than the expected arrival time spread $\Delta\tau$ of the transmission, which in fact constitutes a fundamental condition for the choice of L for a given T and $\Delta\tau$. It can be additionally shown that the output of modulation introduced by Eq.(A.I.5) introduces no self-clutter in the time domain even for matched filtering.

Appendix II

Primitive polynomials

Primitive polynomials can be calculated using the `primpoly.m` function of Matlab's Signal Communication Toolbox. Additionally, many references contain tables of primitive polynomials $h(x)$ for different orders r, althoug an extensive list of all possible polynomials for a given r is rarely indicated due to the fast grow of the number of polynomials as r increases (see Fig.6.1). An efficient and compact way to present a table of primitive polynomials is to represent only the powers which contain the coefficients h_i equal to one. In this way, the polynomial $h(x) = x^{12} + x^9 + x^3 + x^2 + 1$ is represented simply as $[12, 9, 3, 2, 0]$. This is the notation which is going to be used in the following list of primitive polynomials.

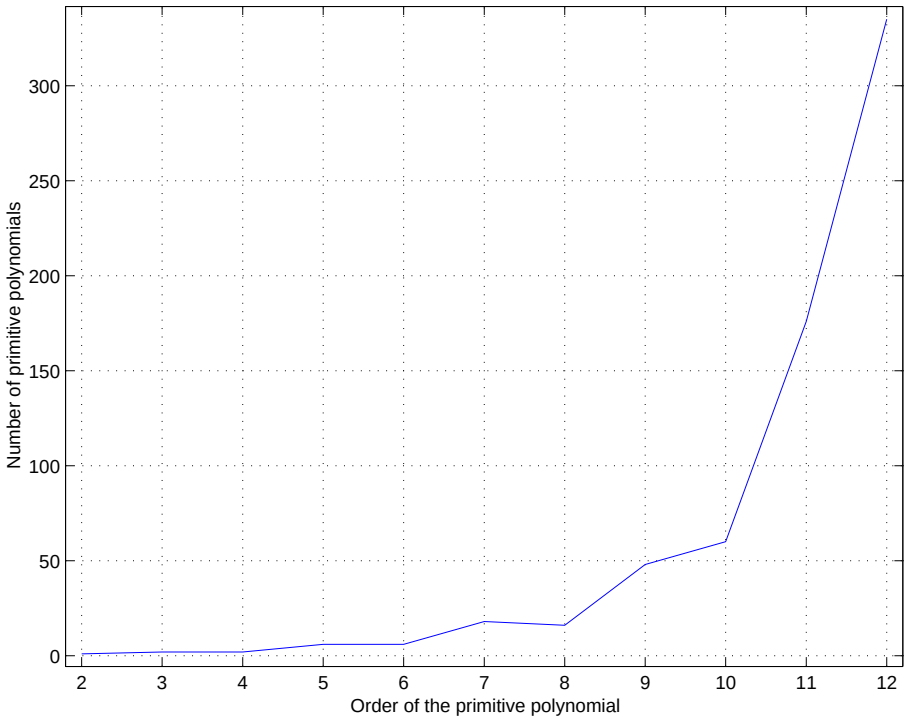

Figure 6.1: Dependence of the number of primitive polynomials, N, on the polynomials order, r.

List of primitive polynomials:

$r = 2$ ($N = 1$): $[2, 1, 0]$.

$r = 3$ ($N = 2$): $[3, 2, 0]$, $[3, 1, 0]$.

$r = 4$ ($N = 2$): $[4, 3, 0]$, $[4, 1, 0]$.

$r = 5$ ($N = 6$): $[5, 4, 3, 2, 0]$, $[5, 4, 3, 1, 0]$, $[5, 4, 2, 1, 0]$, $[5, 3, 2, 1, 0]$, $[5, 3, 0]$, $[5, 2, 0]$.

$r = 6$ ($N = 6$): $[6, 5, 4, 1, 0]$, $[6, 5, 3, 2, 0]$, $[6, 5, 2, 1, 0]$, $[6, 5, 0]$, $[6, 4, 3, 1, 0]$, $[6, 1, 0]$.

$r = 7$ ($N = 18$): $[7, 6, 5, 4, 3, 2, 0]$, $[7, 6, 5, 4, 2, 1, 0]$, $[7, 6, 5, 3, 2, 1, 0]$, $[7, 6, 5, 2, 0]$, $[7, 6, 5, 4, 0]$, $[7, 6, 4, 2, 0]$, $[7, 6, 4, 1, 0]$, $[7, 6, 3, 1, 0]$, $[7, 6, 0]$, $[7, 5, 4, 3, 2, 1, 0]$, $[7, 5, 4, 3, 0]$, $[7, 5, 3, 1, 0]$, $[7, 5, 2, 1, 0]$, $[7, 4, 3, 2, 0]$, $[7, 4, 0]$, $[7, 3, 2, 1, 0]$, $[7, 3, 0]$, $[7, 1, 0]$.

$r = 8$ ($N = 16$): $[8, 7, 6, 5, 4, 2, 0]$, $[8, 7, 6, 5, 2, 1, 0]$, $[8, 7, 6, 3, 2, 1, 0]$, $[8, 7, 6, 1, 0]$, $[8, 7, 5, 3, 0]$, $[8, 7, 3, 2, 0]$, $[8, 7, 2, 1, 0]$, $[8, 6, 5, 4, 0]$, $[8, 6, 5, 3, 0]$, $[8, 6, 5, 2, 0]$, $[8, 6, 5, 1, 0]$, $[8, 6, 4, 3, 2, 1, 0]$, $[8, 6, 3, 2, 0]$, $[8, 5, 3, 2, 0]$, $[8, 5, 3, 1, 0]$, $[8, 4, 3, 2, 0]$.

$r = 9$ ($N = 48$): $[9, 8, 7, 6, 5, 4, 3, 1, 0]$, $[9, 8, 7, 6, 5, 3, 0]$, $[9, 8, 7, 6, 5, 1, 0]$, $[9, 8, 7, 6, 4, 3, 0]$, $[9, 8, 7, 6, 4, 2, 0]$, $[9, 8, 7, 6, 3, 2, 0]$, $[9, 8, 7, 6, 3, 1, 0]$, $[9, 8, 7, 6, 2, 1, 0]$, $[9, 8, 7, 5, 4, 3, 0]$, $[9, 8, 7, 5, 4, 2, 0]$, $[9, 8, 7, 3, 2, 1, 0]$, $[9, 8, 7, 2, 0]$, $[9, 8, 6, 5, 4, 3, 2, 1, 0]$, $[9, 8, 6, 5, 4, 1, 0]$, $[9, 8, 6, 5, 3, 2, 0]$, $[9, 8, 6, 5, 3, 1, 0]$, $[9, 8, 6, 5, 0]$, $[9, 8, 6, 4, 3, 1, 0]$, $[9, 8, 6, 3, 2, 1, 0]$, $[9, 8, 5, 4, 3, 1, 0]$, $[9, 8, 5, 4, 0]$, $[9, 8, 5, 1, 0]$, $[9, 8, 4, 3, 2, 1, 0]$, $[9, 8, 4, 2, 0]$, $[9, 8, 4, 1, 0]$, $[9, 7, 6, 5, 4, 3, 0]$, $[9, 7, 6, 5, 4, 2, 0]$, $[9, 7, 6, 4, 3, 1, 0]$, $[9, 7, 6, 4, 0]$, $[9, 7, 6, 3, 2, 1, 0]$, $[9, 7, 5, 4, 3, 2, 0]$, $[9, 7, 5, 4, 2, 1, 0]$, $[9, 7, 5, 2, 0]$, $[9, 7, 5, 3, 2, 1, 0]$, $[9, 7, 5, 1, 0]$, $[9, 7, 4, 2, 0]$, $[9, 7, 2, 1, 0]$, $[9, 6, 5, 4, 3, 2, 0]$, $[9, 6, 5, 4, 2, 1, 0]$, $[9, 6, 5, 3, 2, 1, 0]$, $[9, 6, 5, 3, 0]$, $[9, 6, 4, 3, 0]$, $[9, 6, 4, 3, 2, 1, 0]$, $[9, 5, 4, 1, 0]$, $[9, 5, 3, 2, 0]$, $[9, 5, 0]$, $[9, 4, 3, 1, 0]$, $[9, 4, 0]$.

$r = 10$ ($N = 60$): $[10, 9, 8, 7, 6, 5, 4, 3, 0]$, $[10, 9, 8, 7, 6, 5, 4, 1, 0]$, $[10, 9, 8, 7, 4, 1, 0]$, $[10, 9, 8, 7, 3, 2, 0]$, $[10, 9, 8, 7, 6, 4, 3, 1, 0]$, $[10, 9, 8, 7, 5, 4, 0]$, $[10, 9, 8, 6, 5, 4, 3, 2, 0]$, $[10, 9, 8, 6, 5, 1, 0]$, $[10, 9, 8, 6, 4, 3, 0]$, $[10, 9, 8, 6, 4, 2, 0]$, $[10, 9, 8, 6, 3, 2, 0]$, $[10, 9, 8, 6, 2, 1, 0]$, $[10, 9, 8, 5, 4, 3, 0]$, $[10, 9, 8, 5, 0]$, $[10, 9, 8, 4, 3, 2, 0]$, $[10, 9, 8, 4, 2, 1, 0]$, $[10, 9, 7, 6, 5, 4, 3, 2, 0]$, $[10, 9, 7, 6, 4, 3, 2, 1, 0]$, $[10, 9, 7, 6, 4, 1, 0]$, $[10, 9, 7, 6, 0]$, $[10, 9, 7, 5, 4, 2, 0]$, $[10, 9, 7, 3, 0]$, $[10, 9, 6, 5, 4, 3, 2, 1, 0]$, $[10, 9, 6, 5, 4, 3, 0]$, $[10, 9, 6, 4, 3, 1, 0]$, $[10, 9, 6, 3, 2, 1, 0]$, $[10, 9, 6, 1, 0]$, $[10, 9, 5, 4, 2, 1, 0]$, $[10, 9, 5, 2, 0]$, $[10, 9, 4, 1, 0]$, $[10, 9, 4, 2, 0]$, $[10, 8, 7, 6, 5, 4, 3, 1, 0]$, $[10, 8, 7, 6, 5, 4, 2, 1, 0]$, $[10, 8, 7, 6, 5, 2, 0]$, $[10, 8, 7, 6, 2, 1, 0]$, $[10, 8, 7, 5, 0]$, $[10, 8, 7, 4, 2, 1, 0]$, $[10, 8, 7, 3, 2, 1, 0]$, $[10, 8, 7, 2, 0]$, $[10, 8, 6, 5, 3, 1, 0]$, $[10, 8, 6, 4, 2, 1, 0]$, $[10, 8, 6, 1, 0]$, $[10, 8, 5, 4, 3, 2, 0]$, $[10, 8, 5, 4, 0]$, $[10, 8, 5, 1, 0]$, $[10, 8, 4, 3, 0]$, $[10, 8, 3, 2, 0]$, $[10, 7, 6, 5, 4, 3, 2, 1, 0]$, $[10, 7, 6, 5, 4, 1, 0]$, $[10, 7, 6, 5, 2, 1, 0]$, $[10, 7, 6, 4, 2, 1, 0]$, $[10, 7, 6, 2, 0]$, $[10, 7, 3, 1, 0]$, $[10, 7, 0]$, $[10, 6, 5, 3, 2, 1, 0]$, $[10, 6, 5, 2, 0]$, $[10, 5, 3, 2, 0]$, $[10, 5, 2, 1, 0]$, $[10, 4, 3, 1, 0]$,

$[10, 3, 0]$.

$r = 11$ ($N = 176$): $[10, 9, 8, 7, 6, 5, 2, 0]$, $[10, 9, 8, 7, 6, 4, 1, 0]$, $[10, 9, 8, 7, 6, 3, 2, 0]$, $[10, 9, 8, 7, 5, 3, 2, 0]$, $[10, 9, 8, 7, 5, 2, 1, 0]$, $[10, 9, 8, 7, 4, 3, 1, 0]$, $[10, 9, 8, 7, 4, 2, 1, 0]$, $[10, 9, 8, 7, 4, 0]$, $[10, 9, 8, 7, 1, 0]$, $[10, 9, 8, 6, 5, 4, 2, 0]$, $[10, 9, 8, 6, 5, 3, 2, 0]$, $[10, 9, 8, 6, 5, 3, 1, 0]$, $[10, 9, 8, 6, 4, 3, 2, 0]$, $[10, 9, 8, 5, 4, 0]$, $[10, 9, 8, 4, 3, 0]$, $[10, 9, 8, 3, 1, 0]$, $[10, 9, 8, 7, 6, 5, 3, 0]$, $[10, 9, 8, 7, 5, 4, 2, 0]$, $[10, 9, 8, 5, 4, 2, 1, 0]$, $[10, 9, 7, 6, 5, 4, 3, 0]$, $[10, 9, 7, 6, 4, 3, 2, 0]$, $[10, 9, 7, 6, 5, 4, 1, 0]$, $[10, 9, 7, 6, 3, 2, 1, 0]$, $[10, 9, 7, 5, 4, 3, 1, 0]$, $[10, 9, 7, 5, 1, 0]$, $[10, 9, 7, 4, 3, 2, 1, 0]$, $[10, 9, 7, 4, 1, 0]$, $[10, 9, 7, 0]$, $[10, 9, 6, 5, 4, 3, 1, 0]$, $[10, 9, 6, 5, 4, 0]$, $[10, 9, 6, 5, 4, 3, 2, 0]$, $[10, 9, 6, 4, 2, 0]$, $[10, 9, 6, 4, 3, 2, 1, 0]$, $[10, 9, 6, 3, 1, 0]$, $[10, 9, 6, 2, 1, 0]$, $[10, 9, 5, 4, 3, 0]$, $[10, 9, 5, 4, 1, 0]$, $[10, 9, 5, 3, 1, 0]$, $[10, 9, 5, 2, 1, 0]$, $[10, 9, 5, 0]$, $[10, 9, 4, 3, 2, 0]$, $[10, 9, 2, 0]$, $[10, 8, 7, 6, 5, 4, 2, 0]$, $[10, 8, 7, 6, 5, 2, 1, 0]$, $[10, 8, 7, 6, 5, 0]$, $[10, 8, 7, 6, 4, 3, 1, 0]$, $[10, 8, 7, 6, 4, 2, 1, 0]$, $[10, 8, 7, 6, 3, 0]$, $[10, 8, 7, 5, 4, 3, 2, 0]$, $[10, 8, 7, 5, 4, 3, 1, 0]$, $[10, 8, 7, 5, 3, 0]$, $[10, 8, 7, 4, 3, 2, 1, 0]$, $[10, 8, 7, 4, 1, 0]$, $[10, 8, 6, 5, 3, 2, 1, 0]$, $[10, 8, 6, 5, 1, 0]$, $[10, 8, 6, 5, 4, 0]$, $[10, 8, 6, 4, 3, 0]$, $[10, 8, 6, 4, 2, 0]$, $[10, 8, 6, 2, 1, 0]$, $[10, 8, 6, 0]$, $[10, 8, 5, 3, 2, 0]$, $[10, 8, 5, 2, 1, 0]$, $[10, 8, 4, 3, 2, 0]$, $[10, 8, 3, 2, 1, 0]$, $[10, 8, 1, 0]$, $[10, 7, 6, 5, 4, 2, 1, 0]$, $[10, 7, 6, 5, 3, 0]$, $[10, 7, 6, 5, 1, 0]$, $[10, 7, 6, 4, 2, 0]$, $[10, 7, 6, 4, 1, 0]$, $[10, 7, 6, 3, 2, 0]$, $[10, 7, 6, 2, 1, 0]$, $[10, 7, 5, 4, 3, 2, 1, 0]$, $[10, 7, 5, 4, 1, 0]$, $[10, 7, 4, 3, 2, 0]$, $[10, 7, 4, 3, 1, 0]$, $[10, 7, 4, 2, 1, 0]$, $[10, 7, 3, 0]$, $[10, 7, 2, 0]$, $[10, 6, 5, 4, 1, 0]$, $[10, 6, 5, 3, 1, 0]$, $[10, 6, 5, 0]$, $[10, 6, 4, 2, 1, 0]$, $[10, 4, 3, 2, 1, 0]$, $[10, 4, 3, 0]$, $[10, 3, 2, 0]$, $[10, 3, 1, 0]$, $[9, 8, 7, 6, 5, 3, 2, 0]$, $[9, 8, 7, 6, 5, 2, 1, 0]$, $[9, 8, 7, 6, 4, 3, 2, 0]$, $[9, 8, 7, 6, 4, 3, 1, 0]$, $[9, 8, 7, 6, 3, 0]$, $[9, 8, 7, 5, 4, 3, 2, 0]$, $[9, 8, 7, 5, 4, 2, 1, 0]$, $[9, 8, 7, 5, 3, 2, 1, 0]$, $[9, 8, 7, 4, 2, 0]$, $[9, 8, 7, 4, 1, 0]$, $[9, 8, 7, 3, 1, 0]$, $[9, 8, 7, 2, 1, 0]$, $[9, 8, 6, 5, 4, 3, 2, 0]$, $[9, 8, 6, 5, 3, 2, 1, 0]$, $[9, 8, 6, 5, 2, 0]$, $[9, 8, 6, 4, 3, 2, 1, 0]$, $[9, 8, 6, 4, 3, 0]$, $[9, 8, 6, 3, 1, 0]$, $[9, 8, 6, 0]$, $[9, 8, 5, 4, 3, 2, 1, 0]$, $[9, 8, 5, 4, 1, 0]$, $[9, 8, 4, 0]$, $[9, 8, 3, 0]$, $[9, 8, 1, 0]$, $[9, 7, 6, 5, 4, 3, 1, 0]$, $[9, 7, 6, 5, 4, 0]$, $[9, 7, 6, 5, 3, 2, 1, 0]$, $[9, 7, 6, 5, 3, 0]$, $[9, 7, 6, 4, 3, 2, 1, 0]$, $[9, 7, 6, 4, 2, 0]$, $[9, 7, 5, 4, 2, 0]$, $[9, 7, 5, 4, 1, 0]$, $[9, 7, 5, 3, 1, 0]$, $[9, 7, 5, 2, 1, 0]$, $[9, 7, 4, 3, 2, 0]$, $[9, 7, 4, 0]$, $[9, 7, 2, 0]$, $[9, 6, 5, 4, 3, 2, 1, 0]$, $[9, 6, 5, 4, 3, 0]$, $[9, 6, 5, 3, 2, 0]$, $[9, 6, 5, 0]$, $[9, 6, 3, 0]$, $[9, 5, 3, 0]$, $[9, 4, 2, 0]$, $[9, 4, 1, 0]$, $[9, 2, 1, 0]$, $[9, 0]$, $[8, 7, 6, 5, 4, 2, 1, 0]$, $[8, 7, 6, 5, 2, 0]$, $[8, 7, 6, 4, 3, 0]$, $[8, 7, 6, 2, 1, 0]$, $[8, 7, 5, 4, 3, 0]$, $[8, 7, 5, 3, 2, 0]$, $[8, 7, 5, 3, 1, 0]$, $[8, 7, 3, 2, 1, 0]$, $[8, 7, 1, 0]$, $[8, 6, 5, 4, 3, 2, 1, 0]$, $[8, 6, 5, 4, 1, 0]$, $[8, 6, 4, 3, 1, 0]$, $[8, 6, 2, 0]$, $[8, 6, 5, 4, 2, 0]$, $[8, 6, 4,]$, 0 $[8, 6, 3, 0]$, $[8, 5, 4, 3, 2, 0]$, $[8, 5, 4, 3, 1, 0]$, $[8, 5, 3, 0]$, $[8, 5, 2, 0]$, $[8, 4, 1, 0]$, $[8, 3, 2, 0]$, $[7, 6, 5, 4, 2, 0]$, $[7, 6, 5, 3, 1, 0]$, $[7, 6, 5, 2, 1, 0]$, $[7, 6, 5, 0]$, $[7, 6, 4, 0]$, $[7, 6, 3, 2, 1, 0]$, $[7, 5, 4, 0]$, $[7, 5, 3, 0]$, $[7, 4, 3, 2, 1, 0]$, $[7, 4, 2, 0]$, $[7, 3, 2, 0]$, $[6, 5, 4, 3, 1, 0]$, $[6, 5, 4, 0]$, $[6, 5, 2, 0]$, $[6, 5, 1, 0]$, $[6, 2, 1, 0]$, $[5, 3, 2, 0]$, $[5, 3, 1, 0]$, $[4, 2, 1, 0]$, $[2, 0]$.